

# Optimization of “Over-coded” Radar Waveforms

John Jakabosky<sup>1</sup>, Shannon D. Blunt<sup>1</sup>, and Braham Himed<sup>2</sup>

<sup>1</sup>Radar Systems Lab, University of Kansas, Lawrence, KS

<sup>2</sup>Sensors Directorate, Air Force Research Laboratory, Dayton, OH

**Abstract** – Polyphase-Coded FM (PCFM) radar waveforms generated using the power and spectrally efficient continuous phase modulation (CPM) framework can be further enhanced through the use of finer time control by subdividing each phase transition into sub-transitions and by allowing a greater phase excursion per transition interval, herein referred to as over-phasing. These two strategies are denoted collectively as “over-coding”. It is shown that various combinations of sub-transitions and over-phasing can greatly improve waveform design capabilities by expanding the available degrees-of-freedom. It is also demonstrated that the commensurate increase in computational complexity for optimization under the over-coding paradigm can largely be offset through GPGPU processing.

## I. INTRODUCTION

Modern radar systems increasingly require radar emissions that provide both spectral and power efficiency. Power efficiency, enabled by constant modulus waveforms and the use of high power amplifiers operated in saturation, is necessary to achieve radar sensitivity requirements. The need for spectral efficiency is a consequence of electromagnetic compatibility guidelines such as the Radar Spectrum Engineering Criteria (RSEC). The continuous phase modulation (CPM) implementation [1,2] has been shown to be effective at producing polyphase-coded FM (PCFM) waveforms with high spectral efficiency and that are amenable for high power operation. The optimization of PCFM waveforms has been demonstrated [3-5] to facilitate the design of physical radar emissions that even account for the distortion imparted by a high-power transmitter. In this work the underlying CPM implementation is re-examined to discern where additional design freedoms may be exploited.

Denoted as “over-coding”, this generalization of the radar CPM implementation in [1,2] consists of two attributes. First, an increased temporal sampling of the code-to-waveform implementation structure is considered in which the phase transitions, which are themselves derived from the phase values of the chips in the code, are divided into sub-transitions, albeit with a stricter phase-change constraint to avoid increasing the prescribed time-bandwidth product. In contrast, the second attribute considers the allowance of phase transitions that exceed the bound of  $\pm\pi$  (from [1,2]) thereby permitting a possible increase in time-bandwidth product, or at least the design freedoms afforded by occasional excursions beyond the  $\pm\pi$  bound. The prospective benefit of these new sources of design freedom, which arise due to the nature of the CPM radar code-to-waveform implementation, is a greater flexibility for waveform design that becomes particularly important for the realization of complex waveform-diverse operating schemes [6-8].

The possible detractor to this much-increased design freedom is the increased dimensionality dictated by the over-coded CPM implementation which subsequently results in a significant increase in computation for optimization due to the greatly expanded search space. However, available technologies such as parallel processing and general purpose graphic processing unit (GPGPU) computation can greatly aid in offsetting this higher cost.

## II. OVER-CODED CPM IMPLEMENTATION

Continuous Phase Modulation (CPM) has been shown to be effective as a means to implement radar codes as physical, transmitter-amenable PCFM waveforms that are intrinsically constant amplitude and possess tight spectral containment. For greater control over waveform degrees of freedom, this modulation framework is readily modified to support over-coding, the structure of which is comprised of a sub-transition framework for phase changes and an increased freedom for the amount of phase change per transition interval through over-phasing.

The CPM radar code-to-waveform implementation described in [1,2] converted a length  $N+1$  polyphase code comprised of phase values  $\theta_0, \theta_1, \dots, \theta_N$  into a sequence of  $N$  phase-change values via

$$\alpha_n = \begin{cases} \tilde{\alpha}_n & \text{if } |\tilde{\alpha}_n| \leq \pi \\ \tilde{\alpha}_n - 2\text{sgn}(\tilde{\alpha}_n) & \text{if } |\tilde{\alpha}_n| > \pi \end{cases} \quad (1)$$

where

$$\tilde{\alpha}_n = \theta_n - \theta_{n-1} \quad \text{for } n=1, \dots, N. \quad (2)$$

By limiting the maximum phase change to  $\pi$  in (1), this implementation ensures that the phase transition always takes the shortest path around the unit phase circle for the benefit of spectral containment, which is clearly dependent upon the time derivative of phase. Also, noting that while  $\alpha_n$  in (1) represents the amount and direction of the phase change, the path this phase change takes depends on the shaping filter  $g(t)$  that could be rectangular, raised cosine, etc. (see Fig. 1).

The sub-transition representation thus provides a finer granularity for the trajectory of phase changes over a given time interval, essentially allowing for small deviations in the phase trajectory that can translate into improved reduction of range sidelobes. Likewise, relaxation of the maximum phase change of  $\pm\pi$ , at least to a modest degree and for relatively rare occurrences, can provide greater design degrees of freedom with only nominal increase to the spectral footprint.

The CPM framework from [1,2] with modifications to support over-coding is shown in Fig. 1. Dividing each of the original  $N$  phase transition into  $L$  sub-transitions, a weighted

impulse train  $p(t)$  is formed from the resulting  $NL$  total sub-transitions that are now denoted as  $\alpha_{Ln}$ . The impulses are separated by  $T_s$  such that the total pulse width of the waveform is  $T = NL T_s = NT_p$ , where  $T_p$  is the temporal extent of each original phase transition. The shaping filter  $g(t)$ , which integrates to unity over its (now shortened) temporal support of  $[0, T_s]$ , converts the weighted impulse train into a piecewise continuous function that is subsequently integrated to provide continuous phase.

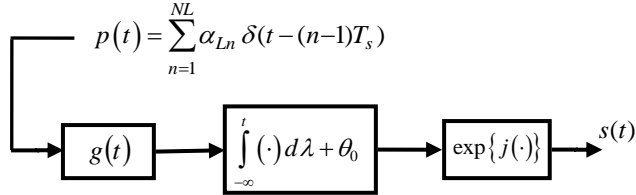


Figure 1. Over-coded CPM Implementation

The  $n^{\text{th}}$  impulse in  $p(t)$  is weighted by the phase-change  $\alpha_{Ln}$  that is defined according to a discrete constellation of possible values on the unit phase circle. For the original CPM radar implementation [1,2],  $\alpha_{Ln}$  could be any one of  $C$  values taken from an equal-partitioned grid on  $[-\pi, +\pi]$ . When using the over-phasing and sub-transition options,  $\alpha_{Ln}$  can be any one of  $MC$  values on an equal-partitioned grid on  $[-M\pi/L, +M\pi/L]$ . Without over-phasing,  $M = 1$  so the  $\alpha_{Ln}$  constellation is comprised of  $C$  equidistant values on  $[-\pi/L, +\pi/L]$ . Likewise,  $L = 1$  indicates no division of the phase transitions.

Here we consider different combinations of  $M = 1, 2$  and  $L = 1, 2, 4, \text{ and } 8$ . The  $(M = 1, L = 1)$  case reduces to the original CPM radar waveform implementation of [1,2] for which we will use an optimized PCFM waveform from [5]. For the other combinations further optimization is required. It is discussed in the next section how the optimization process is performed and straightforward way to initialize a higher-dimensional waveform optimization process using a lower-dimensional optimization result.

### III. OVER-CODED WAVEFORM OPTIMIZATION

The choice of optimization scheme for the radar waveform is arbitrary. The approach used must be able to search a large search space in a reasonable amount of time. The greedy search procedure used in [3-5] is employed here as well. Other approaches may provide better results, or may provide similar results using less computational resources. However, the purpose here is not to compare optimization methods but to demonstrate the feasibility and utility of the over-coded CPM structure for the design of physical waveforms.

The basic approach to this optimization scheme is to determine the best  $\alpha_{Ln}$  from the discrete constellation on  $[-M\pi/L, +M\pi/L]$  independently for each of the  $n = 1, \dots, NL$  sub-transitions, while keeping the other  $NL - 1$  sub-transitions unchanged. Thus the optimization involves  $NL$  parallel search processes before a decision is made to change a single value within the  $\alpha_{Ln}$  sequence.

For the  $n^{\text{th}}$  of  $NL$  parallel searches, a set of  $MC$  candidate waveforms is formed by setting  $\alpha_{Ln}$  to each of the different values in the phase transition constellation and subsequently

generating a new  $s(t)$  using the modified CPM implementation from Fig. 1. The selection of the best value for  $\alpha_{Ln}$  is made by evaluating a metric (e.g. PSL, ISL, etc.) for each resulting candidate  $s(t)$ . Thus each iteration in the optimization process involves determining both the particular sub-transition (indexed by  $n$ ) and its associated best new phase transition value from the available constellation that provides the most improvement for the selected metric. While it is clear that this greedy search strategy can and will encounter local optimality conditions, this limitation can be greatly alleviated by varying the particular assessment metric, a process denoted as *performance diversity* [5], since it is far less likely that the same local optimality locations in the search space will exist across each of the metrics. Note that such a strategy is not the same as multi-objective optimization as all the metrics considered are just different measures of the range sidelobes.

This greedy search procedure was found [5] to be quite tractable for waveform optimization on a search space of size  $C^N$  when  $N$  and  $C$  are each on the order of 100. For example, when  $N = C = 64$ , the space of  $64^{64} \cong 3.9 \times 10^{115}$  possible waveforms has been successfully searched with excellent results [4,5], though the global optimum cannot be guaranteed due to the sheer size of the search space. By comparison, to perform waveform optimization under the over-coding paradigm realizes a search space of  $(MC)^{NL}$  possible waveforms. With  $N = 64, C = 64, M = 2, \text{ and } L = 8$ , the number of possible waveforms is now  $128^{512} \cong 7.8 \times 10^{1078}$ . This enormous expansion of the search space necessitates a short cut to accelerate the optimization process.

To accommodate a search of the sub-transition structure for, say  $L = 2$ , the search is initialized with the optimized waveform structure for an  $L = 1$  search. Specifically,

$$\alpha_{(L=2)(n_2=2n_1-1)} = \alpha_{(L=1)(n_1)} \div 2 \quad (3)$$

and

$$\alpha_{(L=2)(n_2=2n_1)} = \alpha_{(L=1)(n_1)} \div 2 \quad (4)$$

for  $n_1 = 1, \dots, N$  associated with  $L = 1$  and  $n_2 = 1, \dots, 2N$  associated with  $L = 2$ , such that the amount of phase transition is split equally over the sub-transitions. The new sub-transition waveform can then be further optimized from a good initial starting point. While this approach is clearly unlikely to find new waveforms for  $L = 2$  that are radically different from those realized with  $L = 1$ , the search of this portion of the greatly expanded solution space is made more computationally feasible. It is likewise straightforward to expand the  $L = 2$  framework to  $L = 4$  and higher via the same manner as (3) and (4).

Using two general-purpose graphics processing units (GPGPUs) in parallel and implementation parameters  $N = 64, C = 64, M = 1$  or  $2, \text{ and } L = 1, 2, 4, \text{ or } 8$ , these collective search tactics enabled between 40,000 and 100,000 candidate waveforms per second to be evaluated (the range is due to the differences in waveform dimensionality). The total run time for the results shown in the next section took less than 6 hours for the highest dimension result. Even greater dimensionality and/or speed could be achieved with the parallel combination of multiple GPGPUs or cluster nodes.

Finally, for over-phasing freedom it is necessary to prevent the waveform spectral content from expanding beyond some allowable boundary as was previously ensured by the phase transition bound of  $\pm\pi$ . As such, a frequency-domain template is employed to define a mean-square error metric between a prescribed waveform spectrum and the spectral content of the waveform-under-test. This frequency metric, denoted as frequency template error (FTE) [5] is used to further constrain the optimization process and thus ultimately enables a reduction in PSL while limiting out-of-band spectral growth (due to the relationship between autocorrelation and power spectral density). The FTE metric is defined as

$$FTE = \left( \frac{1}{f_H - f_L} \right) \int_{f_L}^{f_H} |Z(f) - U(f)|^2 df \quad (5)$$

where  $U(f)$  is the spectral template and  $Z(f)$  is the spectral content of the waveform-under-test. The limits of integration,  $f_L$  and  $f_H$ , are the minimum and maximum frequencies of interest including out-of-band spectral roll-off. As used here, the spectral template is set by using the spectral content of a baseline waveform for the purpose of preventing the spectral content from deviating too much from a prescribed shape. The spectral template can however take any arbitrary shape such as those previously used to design NLFM waveforms via the principle of stationary phase [9].

The optimization metric used here is an aggregation of those mentioned (PSL, ISL, and FTE) via a weighted geometric mean. The autocorrelation metrics (PSL and ISL) are given a collective weight of  $(1-\mu)$ , and the frequency metric (FTE) is given a weight of  $\mu$ . The two autocorrelation metrics are also geometrically weighted with respect to one another with a weight of  $\varepsilon$  for PSL and a weight of  $(1-\varepsilon)$  for ISL. The resulting aggregate metric is thus

$$\text{Aggregate metric: } \left[ (\text{PSL})^\varepsilon (\text{ISL})^{(1-\varepsilon)} \right]^{(1-\mu)} [\text{FTE}]^\mu \quad (6)$$

where the specific values of  $0 \leq \mu \leq 1$  and  $0 \leq \varepsilon \leq 1$  are varied as the optimization progresses to help avoid local optimality.

#### IV. RESULTS

To demonstrate the optimization of an over-coded PCFM waveform, the PSL-optimized waveform from [5], which corresponds to an  $(L = 1, M = 1)$  CPM implementation, is used for the initialization with the expansion approach described in Sect. III. This initial waveform has  $N = 64$  phase transitions and  $C = 64$  equidistant constellation points on  $[-\pi, +\pi]$ . The optimization was performed using  $L = 2, 4,$  and  $8$  sub-transitions and with over-phasing of  $M = 1$  (none) and  $M = 2$ . The time-bandwidth product for all waveforms (measured using 3 dB bandwidth) is well approximated as  $BT \cong N = 64$ .

For the  $M = 2$  over-phasing cases a frequency metric weight of  $\mu = 0.005$  was incorporated into the search metric for the cases of  $L = 2, 4,$  and  $8$  sub-transitions with the frequency template set using the spectral content of the initial  $(L = 1, M = 1)$  waveform. The optimization was comprised of 550 runs, with each run being performed until the given metric could not further improve, and between runs alternating between the metrics of ISL ( $\varepsilon = 0$ ), PSL ( $\varepsilon = 1$ ), and a mix of

the two ( $0 < \varepsilon < 1$ ). Each run used the prior run result as initialization. The final result with the lowest PSL is shown.

The PSL result for each optimization is shown in Fig. 2. As a general trend the PSL decreases with increasing number of sub-transitions  $L$ . The use of over-phasing produced a much lower PSL, particularly in conjunction with  $L = 8$  sub-transitions. There is clearly diminishing improvement as  $L$  increases, though it is more pronounced when over-phasing is not used. It should be noted that, while these results demonstrate very low PSL levels for waveforms based on  $BT \cong 64$ , it is not known if the globally optimal solution has been attained so further improvement may be still be possible.

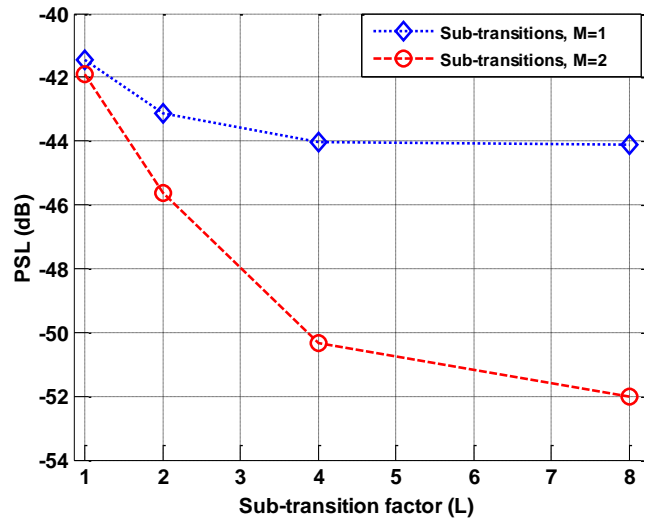


Figure 2. Comparison of PSL for over-coded PCFM waveforms of  $BT \cong 64$  with over-phasing and sub-transitions

A selection of the results of the optimization is shown in Table 1. The initial waveform ( $L = 1, M = 1$ ) is compared against the waveform using only over-phasing ( $L = 1, M = 2$ ), the 8 sub-transition waveform without over-phasing ( $L = 8, M = 1$ ), and the 8 sub-transition waveform with over-phasing ( $L = 8, M = 2$ ).

Table 1. PSL, ISL, and mainlobe half-power width (HPW) for optimized waveforms with  $BT \cong 64$

	$L = 1,$ $M = 1$	$L = 1,$ $M = 2$	$L = 8,$ $M = 1$	$L = 8,$ $M = 2$
<b>PSL (dB)</b>	-41.4	-41.9	-44.1	-52.0
<b>ISL (dB)</b>	-26.1	-27.1	-28.0	-36.9
<b>HPW</b> ( $\times T/N$ )	1.12	1.12	1.11	1.10

All waveforms in Table 1 have PSL values lower than  $-41$  dB and ISL values lower than  $-26$  dB. Thus, as expected, no degradation to PSL or ISL was introduced by over-coding. The ISL values were all close to  $-27$  dB, except for the over-phased, sub-transition waveform ( $L = 8, M = 2$ ), which produced an ISL of  $-36.9$  dB. Such a result is to be expected accompanying the more than 10 dB reduction in PSL observed for this case. All four waveforms maintain a half-power width (HPW) for the autocorrelation mainlobe of around  $1.12 \times T/N$

where  $T$  is the pulsewidth and  $N$  is the number of phase transitions over the pulsewidth. Compared to  $0.88 \times T/N$ , which is found for a CPM-implemented LFM chirp with  $N = 64$ , the mainlobe for these particular examples of nonlinear FM waveforms exhibit only a small degree of degradation in range resolution. More importantly, no further range resolution degradation is observed for over-coding despite the significant further reduction in sidelobe levels.

Full and close-up autocorrelation plots of the initial ( $L = 1, M = 1$ ) and  $L = 8$  sub-transition waveforms (both  $M = 1$  and  $M = 2$ ) are shown in Figs. 3 and 4, respectively. The decrease in ISL and PSL by the sub-transition waveforms is readily apparent. While the HPW of the sub-transition waveforms is marginally smaller than for the initial waveform, the mainlobe for these new waveforms is marginally wider at the  $-50$  dB level.

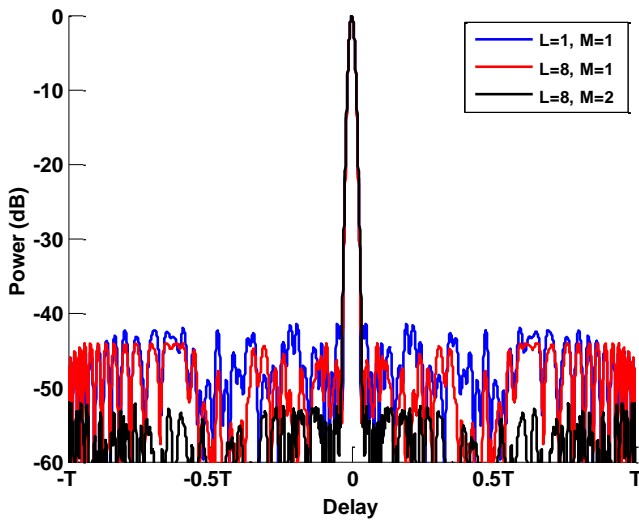


Figure 3. Autocorrelation comparison for over-coded optimized waveforms relative to the non-over-coded optimized waveform ( $BT \cong 64$ )

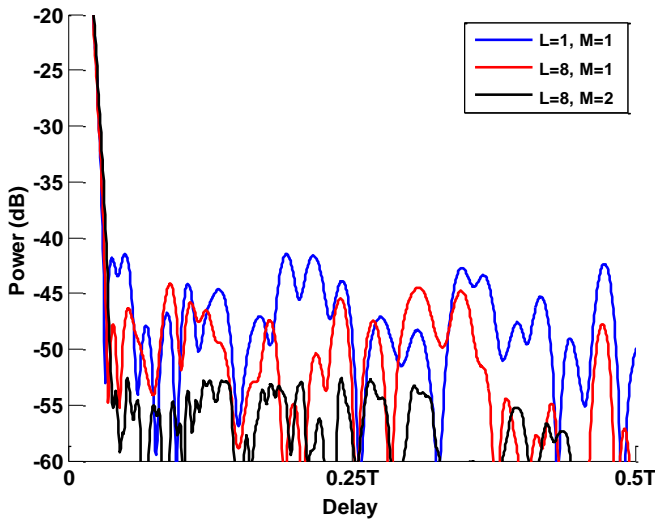


Figure 4. Close-up autocorrelation comparison for over-coded optimized waveforms relative to the non-over-coded optimized waveform ( $BT \cong 64$ )

The respective phase transition values (normalized by  $\pi$ ) for the initial ( $L = 1, M = 1$ ) and sub-transition waveforms

( $L = 8, M = 1$  and  $L = 8, M = 2$ ) are shown in Fig. 5. While the sub-transition waveform sans over-phasing ( $L = 8, M = 1$ ) shows only a minor amount of change relative to the initial waveform due to small sub-transition perturbations, the over-phased waveform ( $L = 8, M = 2$ ) shows significant deviations. These changes manifest primarily in a rapid oscillation of the  $\alpha$  values between positive and negative phase transitions at the beginning and end of the waveform.

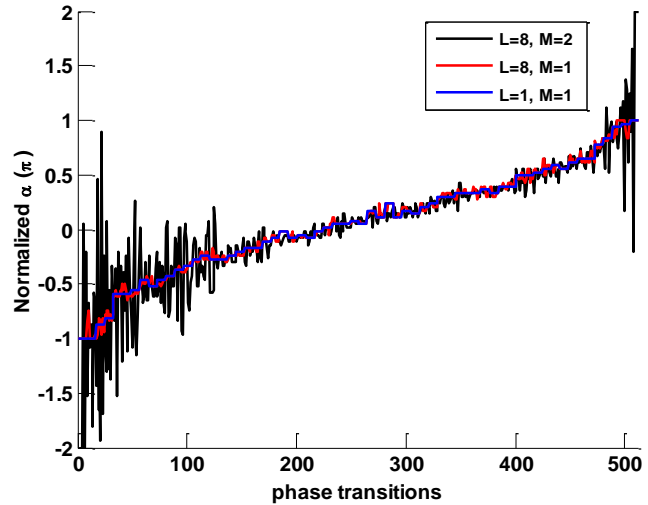


Figure 5. Phase transition ( $\alpha$ ) values comparison for over-coded and non-over-coded waveforms

In Fig. 7 a close-up of selected  $\alpha$  values (top panel) for the initial waveform and an over-coded waveform ( $L = 1, M = 1$  and  $L = 8, M = 1$ ) are compared to the resulting continuous phase trajectories (bottom panel) of each waveform. It is observed that any deviation from the  $\alpha$  values associated with the initial waveform ( $L = 1, M = 1$ ) by the  $L = 8$  sub-transition waveform produces a corresponding deviation in phase for the continuous PCFM waveform.

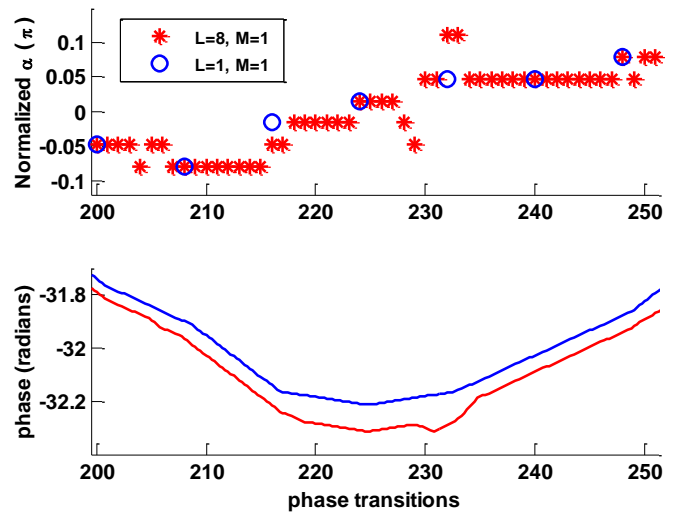


Figure 6. Phase transition ( $\alpha$ ) values compared with unwrapped continuous phase for the the  $L = 1, M = 1$ ; and  $L = 8, M = 2$  waveforms

The spectral content of the initial waveform ( $L = 1, M = 1$ ) and of two versions of over-phased, sub-transition

waveforms ( $L = 4, M = 2$  and  $L = 8, M = 2$ ) is shown in Fig. 6. Above  $-15$  dB the three waveforms are practically identical, while below this point the two over-coded waveforms demonstrate modest spectral spreading. This widening is more evident for the  $L = 8$  sub-transition waveform than the  $L = 4$  sub-transition waveform. Since both of these over-coded waveforms employ over-phasing with  $M = 2$  the frequency metric is needed to prevent the width of the spectral mainlobe from widening significantly (could have potentially doubled without the frequency metric constraint).

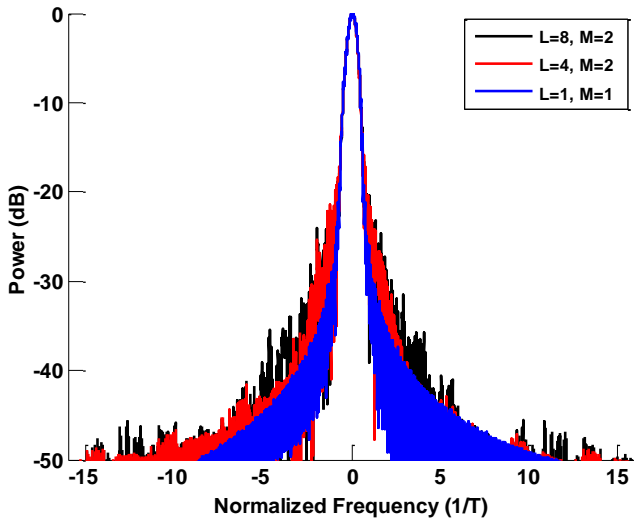


Figure 7. Comparison of waveform spectrum for the  $L = 1, M = 1$ ;  $L = 4, M = 2$ ; and  $L = 8, M = 2$  waveforms

To verify the performance of an over-coded waveform can be realized as a physical emission, a Tektronix AWG70K waveform generator and a Tektronix DPO70K oscilloscope were used. The waveform was implemented on the AWG and then sampled by the oscilloscope (at the rate of 6.25 GS/s). This waveform generator has 10 bits/sample while the oscilloscope has 8 bits/sample. To compensate for noise and signal loss, the waveform generation/sampling was repeated 100 times and coherently integrated. The physical signal was produced at a center frequency of 1.8425 GHz with a total pulse width of  $T = 6.39 \mu\text{s}$ . The autocorrelations of the original and captured signals are shown in Figs. 8 and 9.

Using the ( $L = 8, M = 2$ ) waveform, it was observed that the sampled signal captured by the oscilloscope realized a PSL increase of 2.0 dB, which is rather minimal considering that sidelobes levels still remain below  $-50$  dB for this physical instantiation. Otherwise, the autocorrelation of the captured emission is remarkably close to that of the original waveform, thus verifying that the over-coded waveform can be physically produced. It remains to be seen how this high-dimensional waveform will behave in the presence of the non-ideal/nonlinear distortion that exists in an actual radar system. However, using the “transmitter-in-the-loop” approach from [4,5] in conjunction with over-coding may well enable the increased degrees-of-freedom of the latter to compensate naturally for these deleterious effects of the radar. Furthermore, these degrees-of-freedom may play a significant role in continued efforts to realize transmitter/waveform co-design (e.g. [10]).

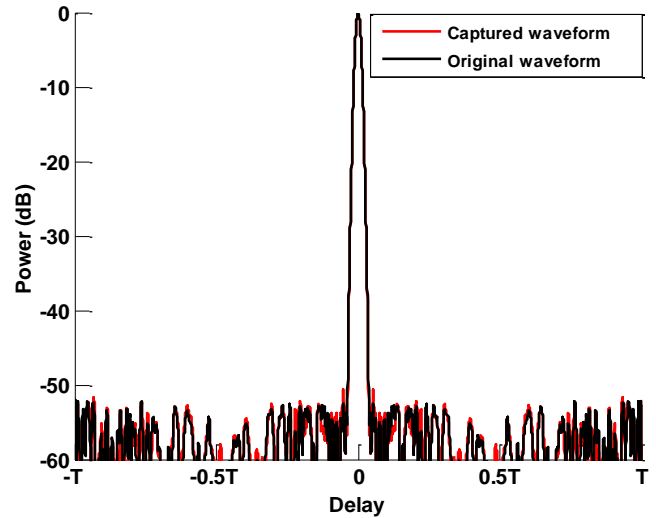


Figure 8. Autocorrelation comparison of the original ( $L = 8, M = 2$ ) waveform with its captured version

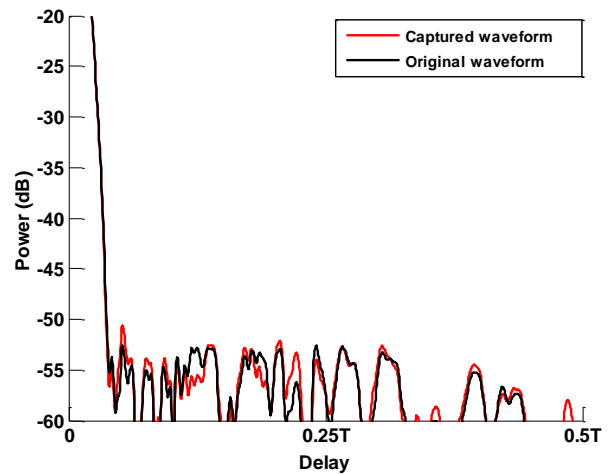


Figure 9. Close-up autocorrelation comparison of the original ( $L = 8, M = 2$ ) waveform with its captured version

Finally, the range-Doppler ambiguity function for the ( $L = 8, M = 2$ ) waveform is shown in Fig. 10. Clearly this over-coded PCFM waveform is similar to other nonlinear FM (NLFM) waveforms in terms of the delay-Doppler coupled mainlobe and surrounding Fresnel lobes. Given the expanded degrees-of-freedom, it may also be possible to trade the improved range sidelobe response at zero Doppler for sidelobe suppression across a non-zero Doppler swath to enhance Doppler tolerance.

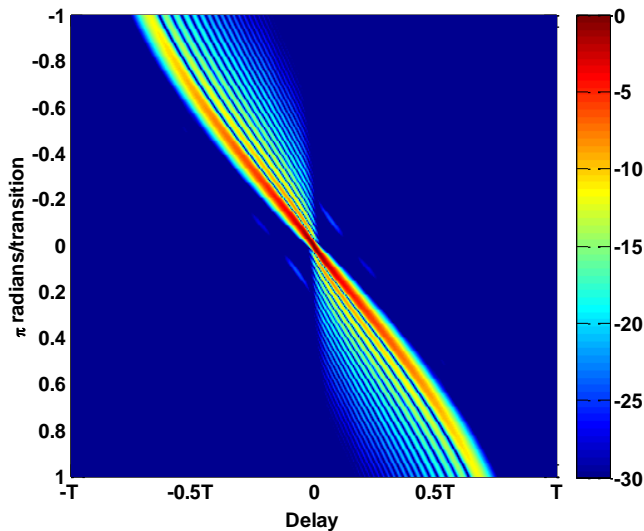


Figure 10. Range-Doppler ambiguity of the  $L = 8, M = 2$  waveform (truncated below  $-30$  dB)

## V. CONCLUSION

A new method of sub-dividing the phase transitions of PCFM waveforms generated within the CPM framework has been demonstrated. An increase in maximum frequency excursion has also been incorporated. These two strategies are collectively referred to as over-coding and allow for greater degrees-of-freedom for the design of physical radar waveforms.

For a time-bandwidth product of approximately 64 and an optimized PCFM waveform based on the original CPM framework possessing  $-41.4$  dB PSL, the additional degrees-of-freedom allowed by over-coding has enabled the realization of a  $-52$  dB PSL waveform with the same time-bandwidth product. Further, such over-coded waveforms have been shown to be amenable to physical generation with an arbitrary

waveform generator, possess the Doppler characteristics typical to NLFM waveforms, and maintain good spectral containment. Ongoing work includes extending the optimization of the autocorrelation response to the range-Doppler response, inclusion of hardware distortion effects, and evaluation of alternative optimization methods.

## REFERENCES

- [1] S.D. Blunt, M. Cook, E. Perrins, and J. de Graaf, "CPM-based radar waveforms for efficiently bandlimiting a transmitted spectrum," *IEEE Radar Conf.*, Pasadena, CA, 4-8 May 2009.
- [2] S.D. Blunt, M. Cook, J. Jakobosky, J. de Graaf, and E. Perrins, "Polyphase-coded FM (PCFM) radar waveforms, part I: implementation," to appear in *IEEE Trans. Aerospace & Electronic Systems*.
- [3] J. Jakobosky, P. Anglin, M.R. Cook, S.D. Blunt, and J. Stiles, "Non-linear FM waveform design using marginal Fisher's information within the CPM framework," *IEEE Radar Conference*, pp. 513-518, May 2011.
- [4] J. Jakobosky, S.D. Blunt, M.R. Cook, J. Stiles, and S.A. Seguin, "Transmitter-in-the-loop optimization of physical radar emissions," *IEEE Radar Conference*, pp. 874-879, May 2012.
- [5] S.D. Blunt, J. Jakobosky, M. Cook, J. Stiles, S. Seguin, and E.L. Mokole, "Polyphase-coded FM (PCFM) radar waveforms, part II: optimization," to appear in *IEEE Trans. Aerospace & Electronic Systems*.
- [6] M. Wicks, E. Mokole, S. Blunt, R. Schneible, and V. Amuso, *Principles of Waveform Diversity & Design*, SciTech Publishing, 2010.
- [7] S. Pillai, K.Y. Li, I. Selesnick, and B. Himed, *Waveform Diversity: Theory & Applications*, McGraw-Hill, 2011.
- [8] F. Gini, A. De Maio, and L.K. Patton, *Waveform Design and Diversity for Advanced Radar Systems*, IET, 2012.
- [9] W.L. Melvin and J.A. Scheer, eds., *Principles of Modern Radar: Advanced Techniques*, SciTech, 2013, Sect. 2.4.
- [10] L. Ryan, J. Jakobosky, S.D. Blunt, C. Allen, and L. Cohen, "Optimizing polyphase-coded FM waveforms within a LINC transmit architecture," *IEEE Radar Conf.*, Cincinnati, OH, 19-23 May 2014.